



## OPEN

## SUBJECT AREAS:

OPTICAL SENSORS

OPTICAL MATERIALS

NANOPHOTONICS AND  
PLASMONICS

RAMAN SPECTROSCOPY

# A solution to the fabrication and tarnishing problems of surface-enhanced Raman spectroscopy (SERS) fiber probes

Antti Matikainen<sup>1</sup>, Tarmo Nuutinen<sup>2</sup>, Pasi Vahimaa<sup>1</sup> & Seppo Honkanen<sup>1</sup><sup>1</sup>Institute of Photonics, University of Eastern Finland, P.O. Box 111, FI-80101 Joensuu, Finland, <sup>2</sup>Department of Biology, University of Eastern Finland, P.O. Box 111, FI-80101 Joensuu, Finland.Received  
28 September 2014Accepted  
14 January 2015Published  
9 February 2015Correspondence and  
requests for materials  
should be addressed to  
T.N. (tarmo.nuutinen@  
uef.fi)

Surface enhanced Raman scattering (SERS) fiber probes have enormous potential in optical sensing applications. However, their widespread use has been hindered by two major obstacles: the difficulty of fabricating the required silver nanostructures on optical fibers and the tarnishing of silver, rapidly degrading their sensing properties. Here we propose a solution to these dilemmas by abandoning the use of metallic silver and conventional nanofabrication procedures. Instead, we base our fabrication on chemically stable silver chloride and show that it can be directly grown on the optical fibers without any advanced fabrication equipment. As silver chloride itself is not SERS-active, we demonstrate how to “activate” the probes by turning the crystals into metallic silver nanostructures via photoreduction. We verify that if stored in the non-activated stage, the sensing properties of the structures remain unchanged. Finally, we demonstrate the high sensitivity (signal-to-noise ratio up to  $42 \pm 3$  dB) of the probes in real-time *in situ* measurements at nanomolar analyte concentrations.

Raman scattering is a phenomenon where light interacts with the molecular structure of a material, which results in photons scattering with altered energies<sup>1</sup>. Since the energy shifts are distinctive for all molecules, Raman spectroscopy enables the chemical composition of a sample to be both qualitatively and quantitatively analyzed. Unfortunately, Raman scattering is a weak phenomenon and thus not directly observable at low analyte concentrations. One of the most widely used method to enhance Raman signal is the so called surface enhanced Raman spectroscopy (SERS)<sup>2</sup>. In SERS, the studied sample is deposited on a nanostructured metal surface (SERS substrate) which interacts with the excitation light that excites localized surface plasmons (LSPs) at the metal/dielectric interface. The LSPs induce a local electromagnetic field enhancement that significantly increases the intensity of Raman scattering originating from the sample molecules. The enhancement is proportional to the fourth power<sup>2</sup> of the electric field  $|E|$  and close to the LSP resonance wavelength,  $|E|$  is greatest in the so called “hot spots” that are located in the immediate vicinity of the metal surface and in the small gaps and cavities between neighbouring metal structures.

SERS has interesting applications in medical diagnostics<sup>3</sup>, where it has been applied to detection of biochemical components related to prostate cancer<sup>4</sup> and Alzheimer’s disease<sup>5</sup>, for example. The applicability of SERS in this field can be further improved by combining the plasmonic SERS nanostructures with an optical fiber, which allows one to perform SERS measurements both *in situ* and *in vivo*. Unlike planar substrates, fabricating probes and creating the required nanostructures on a fiber tip is not straightforward. The lithographic processes<sup>6</sup> that are well suited for fabrication of planar SERS substrates are often poorly compatible with non-planar substrates, such as optical fibers. So far, immobilizing nanoparticles on a fiber tip by dip-and-dry method has been the simplest method to fabricate SERS probes. However, firmly attaching the particles on the fiber tip requires additional fabrication steps, such as silanization<sup>7</sup> and vacuum evaporation coating<sup>8</sup>, which again complicate the fabrication process.

Both in case of planar substrates and fiber probes, silver is often preferred due to its low price and superior scattering properties<sup>9</sup>. Unfortunately, silver is not chemically inert but tends to tarnish, i.e. react with atmospheric gases, such as oxygen and different compounds of sulfur. Due to tarnishing, plasmon resonance dampens and shifts<sup>10</sup>, which leads to a decreased energy density at the metal/dielectric interface. This in turn decreases the Raman signal enhancement, which reduces the measurement sensitivity. One way to prevent tarnishing is to coat the metal with an inert material, such as aluminum oxide<sup>11</sup>. However, as the electromagnetic field amplitude decays exponentially as a function of distance from the metal, even a protective layer of a few nanometers reduces



the enhancement properties by orders of magnitude<sup>12</sup>. Thus, also the measurement sensitivity significantly reduces, which makes this kind of an approach rather futile.

Instead of artificially coating the silver structures, another approach is the use of silver chloride (AgCl). Silver chloride itself cannot be used for SERS but it acts as an intermediate product, which is tarnishing-resistant and can be turned into metallic silver via photoreduction. Thus until chlorine is released during the photoreduction, tarnishing is determined by the properties of silver chloride rather than those of metallic silver, which ensures that fresh silver is always available when needed. Previous attempts, however, where AgCl crystals were precipitated by mixing solutions of sodium chloride and silver nitrate together<sup>13</sup> are not suitable for SERS probe fabrication because the crystals need to be separately extracted from the liquid. This makes the practical implementation of pre-precipitated crystals extremely difficult, as transferring and securely attaching the crystals on a sub-millimeter fiber tip end facet is practically impossible.

Here, we demonstrate how to simultaneously overcome both the tarnishing problem and the problem of fabricating SERS structures on non-planar substrates. Instead of using nanoparticles, lithographic techniques, or pre-precipitated AgCl crystals, we apply a liquid phase thin film deposition method to grow silver chloride directly on the fiber tips. The method is applicable to objects of different shapes and dimensions, which we demonstrate by coating both optical fibers and silicon wafers. We characterize the coatings and show how the AgCl coated optical fibers and silicon wafers can be conveniently activated and turned into SERS probes and planar SERS substrates *in situ*. For the activation and measurements, we use a standard Raman measurement system and we describe how the activation affects the morphology of the silver chloride crystals and how these changes relate to the SERS enhancement of the resulting silver structures. We evaluate the performance of the SERS structures and show the importance of controlling the process in terms of signal enhancement and measurement repeatability. We apply the fabricated SERS probe sensors for monitoring molecular adsorption in real-time. Finally, we demonstrate the extended shelf-life of the non-activated AgCl substrates.

## Results

**Fabrication.** Silver chloride coating process takes place by repeatedly submerging the object to be coated in precursor solutions of silver nitrate (AgNO<sub>3</sub>) and sodium chloride (NaCl) in a cyclic manner in ambient laboratory conditions. This results in Ag<sup>+</sup> and Cl<sup>-</sup> ions nucleating and forming AgCl crystals on the surface of the submerged object. The growth is controlled simply by varying the number of submersion cycles while keeping other parameters, such as the cycle duration and concentrations constant. Here, we coated both silica fibers and silicon wafers with AgCl in 25, 50 and 100 cycles. Silicon wafers were chosen as a reference material for two reasons: firstly, the crystals can be imaged non-invasively with a Scanning electron microscope (SEM) without conductive coating and secondly, they can be used in conventional planar SERS measurements. A schematic flow chart, describing the steps from the fabrication to activation and measurements is shown in Figure 1.

**Characterization of AgCl crystal growth.** SEM imaging of the silica fiber tips shows that the AgCl coatings consist of separate silver chloride crystals. With 25 cycles, only a few crystals are visible yet and the ones observable are located in unevenly scattered patches (Fig. 2a–c). In case of 50 and 100 growth cycles, the crystals are already uniformly distributed over the whole surface area. Granulometric analysis (based on SEM images) reveals that for 25 cycles, the crystal size distribution is nearly of Gaussian shape, centered at  $d \sim 55$  nm and for 50 cycles, the distribution is wider and bell shaped and centered at  $d \sim 90$  nm with contribution from

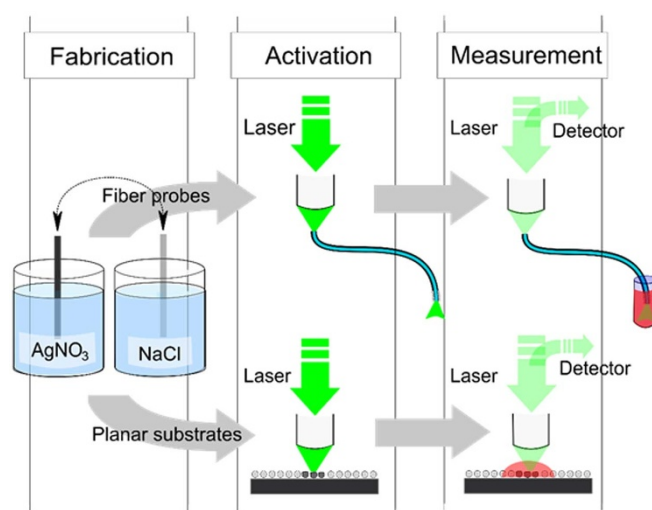


**Figure 1 | Schematic flow chart from the fabrication process to activation and SERS measurements.** After the fabrication, planar SERS substrates are activated and measured with a Raman microscope in a conventional manner while the SERS probes are activated and used in the measurements by coupling the laser light into the fiber using the microscope and recording the signal through the fiber.

the smaller crystals observable as a shoulder around  $d \sim 45$  nm (Fig. 3a). The same shoulder appears also with 100 cycles, but now the maximum has shifted to  $d \sim 120$  nm. Although the crystal number density  $n_c$  (crystals per unit surface area) varies between depositions, the mean diameter  $d_\mu$  clearly shifts towards larger values as the number of growth cycles is increased (Supplementary Table S1). Note that on silica, the crystal diameter is slightly affected by the conductive copper coating.

In the case of planar silicon samples, the crystals were evenly distributed for all deposition cycles (Fig. 2d–f). It is noteworthy that crystals grew larger ( $\sim 50\%$ ) on silicon than on silica fiber end facets but  $n_c$  was now significantly lower and remained relatively constant for all depositions (Supplementary Table S1). Nevertheless, the shape of size distributions for 25, 50 and 100 cycles resemble the corresponding ones on silica samples. For 25 cycles, the shape is close to Gaussian and centered at  $d \sim 80$  nm (Fig. 3b). For 50 cycles, the distribution is again wider and bell shaped (centered at  $d \sim 120$  nm), having contribution from both larger and smaller crystals and a shoulder at  $d \sim 70$  nm. For 100 cycles, the distribution is again Gaussian and centered at 155 nm.

**Activation (photoreduction).** AgCl coated silicon wafers and silica fibers are not SERS-active themselves and need to be reduced into metallic silver in order to unleash the signal enhancing plasmonic properties required for SERS. Activation was achieved by photoreducing the planar samples with the laser of the Raman microscope ( $\lambda = 514$  nm,  $P = 5$  mW and laser exposure duration of 10 minutes). The fiber probes were activated *in situ* in similar fashion: microscope's objective was used to couple the laser beam into the fiber using the same power and the same exposure duration (middle panel in Fig. 1).

A close-up on the individual crystals on a silicon wafer shows that the particle morphology changes significantly during the photoreduction ( $2\text{Ag}^+\text{Cl}^- (\text{s}) \rightarrow 2\text{Ag}^0 (\text{s}) + \text{Cl}_2^0 (\text{g})$ ). Exposure to laser light releases chlorine from the crystal lattice, which results in the collapsing of remaining silver into smaller particles and particle clusters (shown on the right in Fig. 4a–c). Noteworthy, the formation of the structures is dependent on the diameter of the initial crystals: the smallest crystals (25 growth cycles) develop into simple, but separate grains, while the larger crystals (50 and 100 cycles) can

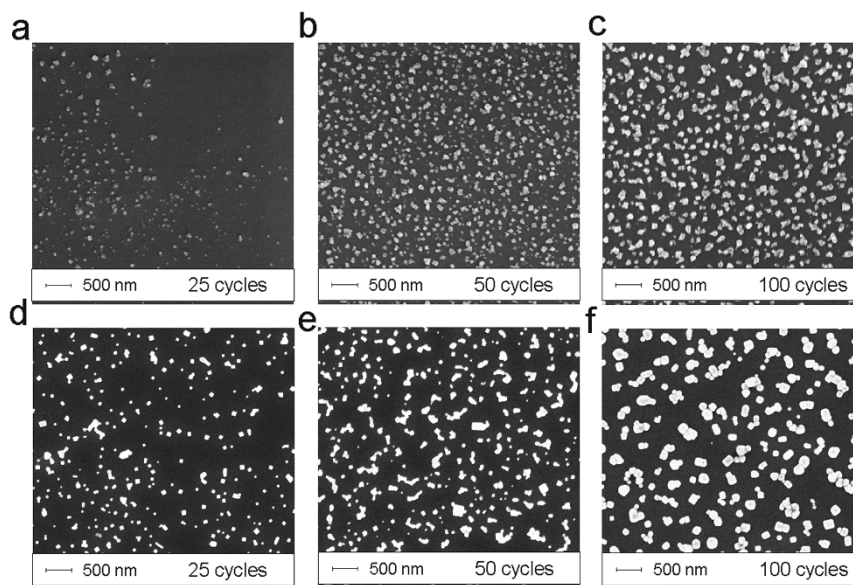


**Figure 2 | Growth of AgCl crystals by SEM.** SEM images of the AgCl crystals grown on optical fiber end facets (a–c) and planar silicon wafers (e–g) with 25 (a,d), 50 (b,e) or 100 (c,f) cycles.

transform into more elaborate nanostructures with splits, gaps and protrusions ranging from a few nanometers to some tens of nanometers in dimension.

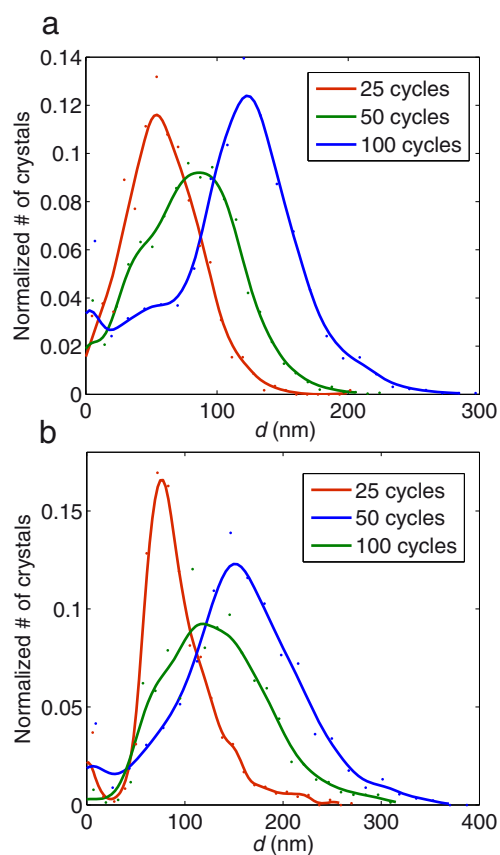


**Figure 3 | Growth of AgCl crystals as normalized size distributions on (a) silica fiber end facets and (b) planar silicon wafers after 25, 50 and 100 growth cycles.** Curve fitting, using the Gaussian Kernel smoother function, is shown for clarity.

**Measurements (Raman signal enhancement).** We first investigated the performance of the planar SERS substrates in terms of Raman signal enhancement. After the activation step and deposition of Rhodamine 6G (Rh6G), a common standard, Raman spectra were recorded from the planar substrates. The spectra, averaged from measurements (excitation wavelength = 514 nm,  $P = 50 \mu\text{W}$ , integration time = 10 s) at 18 different locations, are shown in Fig. 5a. For the activated areas, the major Raman peaks (1311, 1362, 1509, 1575 and  $1650 \text{ cm}^{-1}$ ) all characteristic of Rh6G appeared for all samples of 25, 50 and 100 growth cycles. Using the highest peak at  $1650 \text{ cm}^{-1}$  as an indicator of Raman signal intensity, the signal-to-noise ratio ( $S/N$ ) was calculated for all samples. What is noteworthy is that higher signal-to-noise ratios ( $S/N$ ) were recorded for the samples with a larger initial crystal size:  $S/N = 20 \pm 7$ ,  $S/N = 36 \pm 4$  and  $S/N = 38 \pm 2$  dB were calculated for 25, 50 and 100 growth cycles, respectively. For comparison, a reference measurement recorded from a bare silicon wafer (0 cycles) showed no detectable Raman signal from Rh6G ( $S/N \sim 0$  dB). Similarly, no detectable signals were observed with the non-activated AgCl crystals.

In the SERS fiber probe measurements, Raman microscope was used to couple the excitation light into the fiber and the signal was monitored by placing the probe end of the fiber in an aqueous solution of 200 nM Rh6G and recording the signal through the fiber (right panel in Fig. 1). Using the peak at  $1650 \text{ cm}^{-1}$  again as an indicator, no Raman signal ( $S/N \sim 0$  dB) from Rh6G could be observed for the non-coated reference fiber (0 cycles). This indicates that the concentration was too low for unenhanced Raman measurements (Fig. 5b). However, the probes that were coated and activated, responded to the presence of Rh6G almost instantly. The signal became clearly distinguishable from the noise level ( $S/N > 8$  dB) in approximately five minutes with the probe of 25 cycles and practically immediately in case of 50 and 100 cycles. Vice versa, when a probe was placed in a solution of smaller concentration (20 nM), the signal intensity quickly dropped (Supplementary Fig. S1). During prolonged submersion in 200 nM Rh6G, the signal levels continued to climb for some tens of minutes then began to saturate (Fig. 5c).

Similarly to planar measurements, the signal-to-noise ratio depended again on the number of growth cycles. At the end of the measurements (the last 10 minutes), values of  $S/N = 24 \pm 2$ ,  $S/N = 37 \pm 2$  and  $S/N = 42 \pm 3$  were calculated for the 25, 50 and 100



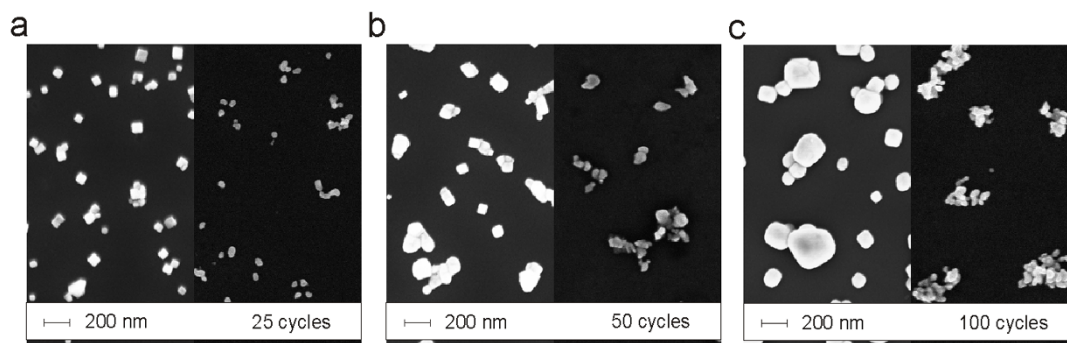


**Figure 4 | Photoinduced collapse of AgCl crystals during the activation.** SEM images with a magnification of  $25k\times$  show the individual crystals grown on silicon wafer in (a) 25, (b) 50 and (c) 100 cycles before (left) and after (right) the activation.

cycles, respectively. Probe sensitivity was further investigated by immersing a probe of 100 cycles in varying concentrations of Rh6G. The lowest concentration, where the signal was still clearly above the noise level ( $S/N = 6 \pm 3$  dB), was 5 nM (Supplementary Fig. S1).

**Shelf-life of AgCl SERS structures.** The shelf life was evaluated using the planar samples. Several samples of 100 growth cycles were stored in the dark but otherwise the samples were exposed to ambient laboratory conditions. Then, the same activation procedure and measurements were repeated after a period of 30, 60 and 120 days. The signal enhancing properties of the SERS substrates remained virtually constant throughout the four month test period

as signals of similar magnitude were obtained for all the measurements (Fig. 5d). Also the calculated signal-to-noise ratios were nearly the same for the fresh and the aged substrates:  $S/N = 38 \pm 3$ ,  $S/N = 39 \pm 2$ ,  $S/N = 42 \pm 3$  and  $S/N = 40 \pm 3$  dB were calculated for the fresh, 30, 60 and 120 days old samples, respectively. In addition, no visual morphological changes that would indicate reduction or tarnishing could be observed in the SEM images of the stored samples.

For comparison, we also investigated how the substrates perform when stored in the activated stage. When stored as metallic silver, the enhancement generated by the structures dropped to approximately one third of the original in just 24 hours (Supplementary Fig. S2).

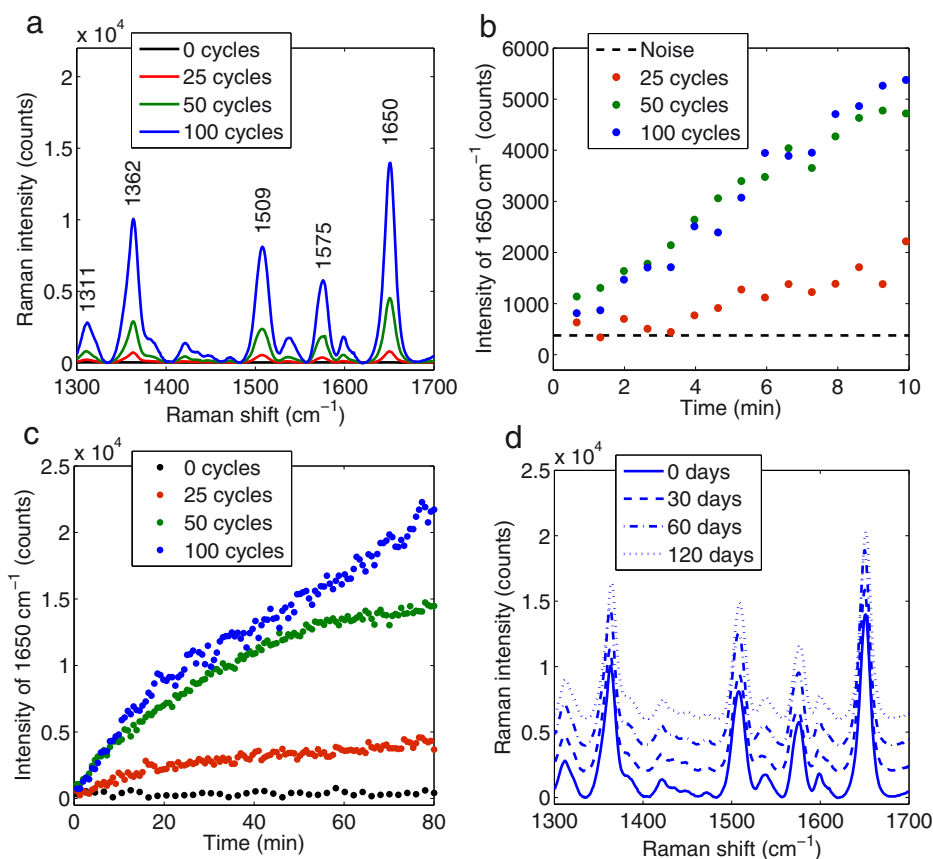


**Figure 5 | Results of the SERS measurements.** (a) Averaged Raman spectra of Rh6G measured from planar SERS substrates. Raman signal evolution in the fiber probe measurements (peak at  $1650\text{ cm}^{-1}$ ) during (b) the first 10 minutes and (c) 80 minutes of immersion in 200 nM Rh6G. (d) Shelf-life measurements (the spectra have been displaced for clarity) for fresh, one month, two months and four months old planar substrates of 100 growth cycles. All the substrates and probes (used in a–d) are photoreduced immediately before the measurements.



## Discussion

The main goal of this study was to demonstrate a feasible method for the fabrication of SERS fiber probes that can be stored for long periods of time without losing their enhancement properties. Since the method is also applicable to planar SERS substrates and the crystals could be more accurately characterized on silicon wafers, we demonstrated both. Besides being a flexible, a unique aspect of the AgCl coating method is that it does not directly produce SERS probes or SERS substrates, but instead, the coating serves as an intermediate product, which is resistant to tarnishing effects of atmospheric gases. Therefore, the signal enhancing silver nanostructures are only preliminarily defined in the deposition process and are actually generated by photons during the activation step that solves the tarnishing problem and is the key to the extended shelf-life of the AgCl based products.

The shelf-life is indeed improved significantly in comparison to metallic silver based products. In addition to our own experiments, it has also previously been shown that dramatic changes in the plasmonic enhancement properties, such as the resonant wavelength and the intensity of the absorption peak, take place within days of exposure to ambient conditions with unprotected metallic silver substrates<sup>10</sup>. Moreover, the tarnishing resistance is further supported by the observation that no tarnishing related morphological changes, which have been reported with metallic silver<sup>14</sup>, could be seen on the non-activated AgCl crystal substrates.

Other advantages of the method are its simplicity, scalability and speed, which are due the simple, single-stepped fabrication process and the use of a liquid phase instead of a gas phase in the deposition. Typically, fabrication of plasmonic nanostructures on a fiber tip requires several fabrication steps e.g. in the case of electron beam patterned<sup>15</sup> and focused ion-beam patterned<sup>16</sup> probes. Also, even if the fabrication can be done in a single step, as in laser ablation patterning<sup>17,18</sup> it can only be applied to one probe at a time. In addition, all gas phase fabrication methods require the use of vacuum pumping. Therefore they are ultimately limited by the dimensions of the vacuum chamber. In the liquid phase, however, no vacuum pumping is needed, and the sizes of the precursor solution containers can be easily up-scaled. Since this and the fact that the AgCl crystal coating requires only inexpensive materials—NaCl, AgNO<sub>3</sub>, water and two containers at the bare minimum—one can easily envision that the SERS fiber probes (and substrates) can be manufactured anywhere in large quantities at very low cost. What separates this method from the previously reported ones that exploit precipitated and collected AgCl crystals<sup>13</sup> is the fact that the crystals can now be directly grown on the substrate, which remarkably simplifies the fabrication. In this way, they can be also applied to arbitrary surfaces, such optical fibers.

In more general context, the fabrication method is not completely unfamiliar, as the process resembles successive ion adsorption and reaction (SILAR)<sup>19</sup>. For some reason, SILAR has gained surprisingly little of academic attention since its invention in the 80's. Perhaps, it mistimed with the “boom” of nanotechnologies and hence many later, more complicated methods became more popular. SILAR can be used in thin film fabrication, where the film thickness has to be controlled with the accuracy of single atomic layer. Typically, in these purposes excessive rinsing steps, elevated temperatures and atmospheric control are employed. However, these requirements are obsolete, as we show here, when the purpose allows slightly higher tolerance in the accuracy. Consequently, by abandoning other requirements than the cyclivity of SILAR (e.g. rinsing steps), fabrication becomes much simpler and extremely fast: the time consumed by the process reduces from several hours<sup>20</sup> to a few minutes. We believe these advantages make our method attractive for many other purposes and applications, where low-cost fabrication of thin films or nanocrystals is required.

The level of control is important also for the fabrication SERS probes and SERS substrates. Although the AgCl crystals are only

an intermediate product in terms of SERS, their distribution and dimensions do affect the performance of the SERS structures. The measurement repeatability is improved as well, as the density of the particles on the surface increases. However, the initial crystal size seems to affect the signal enhancement even more than the amount of the crystals (Supplementary Table S1). This can be explained by how the crystals collapse during the activation step. The larger the initial crystal, the higher occurrence of narrow clefts, pits and protrusions in collapsed silver structures. This leads to higher surface area but more importantly; the higher density of hot spots needed for the SERS.

It should be noted however, that the activation step is not compulsory; if sufficient power is used for the measurements, simultaneous photoreduction can occur. Here we, however, applied the pre-measurement activation step in order to avoid the reduction to metallic silver during the actual measurements, which would have complicated the interpretation of the results. Thus in this case, we can assume that the time course of the increasing signal levels reflects the adsorption dynamics of Rh6G molecules rather than an on-going reduction process. The assumption is supported by the inverse progress when the probe was replaced into a solution of smaller concentration. Similar behavior of signal levels would be likely seen with any other plasmonic probes with freshly made silver nanostructures.

In general, however, it is difficult to compare the performance of different SERS substrates or SERS probes against one another, as the benchmark formula<sup>21</sup> for the enhancement factor (EF) calculation is applicable only to well-defined structures. One way to roughly estimate the enhancement and the measurement sensitivity is to compare the measured target molecule concentration, excitation laser wavelength, power and the required exposure times. In this sense, the sensitivity (5 nM detection limit with S/N of 6) of our probes is more than comparable to the previously discussed metallic silver probes<sup>7</sup>, where detection limit of 200 nM was reported for Rh6G (with excitation wavelength = 633 nm and  $P = 4.5$  mW). In our case though, with the excitation wavelength of 514 nm, we might also benefit from the Resonance Raman (RR) effect<sup>22</sup>. However, as we did not observe any Raman signal from the reference samples, we believe that SERS is predominantly responsible for the total enhancement. Anyway, to the best of our knowledge, detection limits as low as 5 nM (for liquid Rh6G) have not been reported earlier with any SERS fiber probe sensors.

In conclusion, we have demonstrated a facile approach for the fabrication of SERS probes (and substrates), where we exploited the stability of silver chloride crystals for overcoming the notorious tarnishing properties of metallic silver. We showed that AgCl crystals can be activated/reduced to metallic silver using a standard Raman microscope. When stored in the intermediate, non-activated stage, the signal enhancing properties of the AgCl based products remain constant for at least four months. Furthermore, we demonstrated that the mean diameter of the crystals can be controlled by simply varying the number of growth cycles and that the diameter of the initial crystal dictates the morphologies of the photoreduced silver nanostructures. This in turn determines the number of hot spots; the signal enhancement properties and the sensitivity of the fabricated probes and substrates. Furthermore, as the fabrication method of the SERS structures with this method is extremely simple and can be performed anywhere and by anyone, we believe that the method brings SERS one step closer to practical applications and can benefit all kinds of fields of research, where label-free, *in situ* chemical analysis is desired.

## Methods

**Fabrication of planar substrates and fiber probes.** The planar substrates were prepared by cutting 2" single side polished silicon wafer (purchased from Si-Mat, <100>) into pieces of approximately  $0.25 \times 5 \times 50$  mm<sup>3</sup>. The fiber probes were prepared by stripping silica fibers (VIS-NIR,  $l = 1$  m and  $d_{\text{core}} = 90$  μm core



purchased from Oplatek) of their polymer coatings from both ends at a length of approximately 2 cm and then cleaving the end facets.

Both planar silicon substrates and optical fiber probes were fabricated by dipping the objects in 500 ml beakers of 5 mM NaCl (Sigma-Aldrich, <99.8%) and 5 mM AgNO<sub>3</sub> (Sigma-Aldrich, <99% purity). The dipping was done manually in ambient laboratory conditions (room temperature, standard lighting and humidity). Approximate duration of one cycle was 1.5 s. Finally, both substrates and probes were rinsed with water and blown dry with air.

**SEM imaging and granulometric image analysis.** SEM images were taken with an SEM Leo 1550 Gemini scanning electron microscope with an acceleration voltage of 5 kV and magnification of 25000. For fiber tip imaging, the samples were sputter coated with approximately 7 nm layer of copper. Planar substrates were imaged at the polished side of the silicon wafers without conductive copper coating.

Size distributions and crystal number densities were determined using a software originally designed for cell size analysis (CellProfiler<sup>23</sup>) on SEM images, which were contrast enhanced prior to calculations. For each sample, size distributions were calculated using three SEM images from randomly selected locations, containing a total of  $n = 1192$ ,  $n = 733$ , and  $n = 915$  crystals on the silicon wafers and  $n = 584$ ,  $n = 3542$ , and  $n = 2279$  crystals on the optical fiber end faced for 25, 50 and 100 dipping cycles, respectively. The Gaussian Kerner smoother<sup>24</sup> was used in the size distribution figures for visualization purposes.

**Sample preparation, Raman measurements and data processing.** The activation and all measurements were performed using an inVia Raman microscope with a 514 nm excitation laser (20× objective, NA = 0.40). For the planar samples, the activation was achieved by exposing the crystals to laser radiation for 10 minutes at a power of 5 mW and a spot diameter of 20 μm (measured from the CCD camera image of the Raman microscope).

After the activation step, all planar samples were incubated in the target molecule solution (1.0 μM Rh6G) for 20 minutes, rinsed with water and allowed to dry. For the actual measurements, the power, exposure time and spot diameter were reduced to 50 μW, 10 s and 5 μm and 18 measurements were recorded for each sample at different locations. The spectra were baseline corrected using asymmetric least squares smoothing and then averaged.

In the remote measurements, the Raman microscope was used to couple light into the fiber and the activation was performed with the same input power and exposure time as in case of the planar sample measurements. Raman spectra were recorded through the fiber for the duration of 80 minutes from a 200 nM aqueous solution of Rh6G at a power of 0.25 mW and an exposure time of 20 s at intervals of 45 s and then baseline corrected. The same measurement parameters were used also in the detection limit evaluation.

Signal-to-noise ratios were calculated using the equation

$$\frac{S}{N} = 20 \log_{10} \left( \frac{A_{\text{signal}}}{A_{\text{noise}}} \right), \quad (1)$$

where  $A_{\text{signal}}$  is the measured intensity at 1650 cm<sup>-1</sup> and  $A_{\text{noise}}$  is the intensity of the noise. The noise intensity was defined as a root mean square at 1675–1690 cm<sup>-1</sup>, where no Raman peaks were observed.

1. Le Ru, E. & Etchegoin, P. in *Principles of Surface Enhanced Raman Spectroscopy and related plasmonic effects* [29–120] (Elsevier, Amsterdam, 2008).
2. Moskovits, M. in *Surface-Enhanced Raman Scattering: Physics and Applications* [Kneipp, K., Moskovits, M. & Kneipp, H. (ed.)] [1–17] (Springer, Berlin, 2006).
3. Xie, W. & Schlücker, S. Medical applications of surface-enhanced Raman scattering. *Phys. Chem. Chem. Phys.* **15**, 5329–5344 (2013).
4. Yan, B. & Reinhard, B. M. Identification of Tumor Cells through Spectroscopic Profiling of the Cellular Surface Chemistry. *J. Phys. Chem. Lett.* **1**, 1595–1598 (2010).
5. Chou, I. *et al.* Nanofluidic biosensing for beta-amyloid detection using surface enhanced Raman spectroscopy. *Nano Lett.* **8**, 1729–1735 (2008).
6. Fan, M., Andrade, G. F. S. & Brolo, A. G. A review on the fabrication of substrates for surface enhanced Raman spectroscopy and their applications in analytical chemistry. *Anal. Chim. Acta* **693**, 7–25 (2011).
7. Andrade, G. F., Fan, M. & Brolo, A. G. Multilayer silver nanoparticles-modified optical fiber tip for high performance SERS remote sensing. *Biosens. Bioelectron.* **25**, 2270–2275 (2010).
8. David, L. S. & Vo-Dinh, T. Development of an integrated single-fiber SERS sensor. *Sens. Actuators B Chem.* **69**, 28–36 (2000).

9. Baek, S. *et al.* Plasmonic Forward Scattering Effect in Organic Solar Cells: A Powerful Optical Engineering Method. *Sci. Rep.* **3**, 1726; DOI:10.1038/srep01726 (2013).
10. McMahon, M. D., Lopez, R., Meyer, H. M., III, Feldman, L. C. & Haglund, R. F., Jr. Rapid tarnishing of silver nanoparticles in ambient laboratory air. *Appl. Phys. B* **80**, 915–921 (2005).
11. John, J. F., Mahurin, S., Dai, S. & Sepaniak, M. J. Use of atomic layer deposition to improve the stability of silver substrates for in situ, high-temperature SERS measurements. *J. Raman Spectrosc.* **41**, 4–11 (2010).
12. Chervinskii, S., Matikainen, A., Dergachev, A., Lipovskii, A. A. & Honkanen, S. Out-diffused silver island films for surface-enhanced Raman scattering protected with TiO<sub>2</sub> films using atomic layer deposition. *Nanoscale research letters* **9**, 398 (2014).
13. Gan, Z. *et al.* A facile strategy for obtaining fresh Ag as SERS active substrates. *J. Colloid Interface Sci.* **366**, 23–27 (2012).
14. Gorkunov, M. V., Artemov, V. V., Yudin, S. G. & Palto, S. P. Tarnishing of silver subwavelength slit gratings and its effect on extraordinary optical transmission. *Phot. Nano. Fund. Appl.* **14**, 122–129 (2014).
15. Lin, Y., Zou, Y., Mo, Y., Guo, J. & Lindquist, R. G. E-Beam Patterned Gold Nanodot Arrays on Optical Fiber Tips for Localized Surface Plasmon Resonance Biochemical Sensing. *Sensors* **10**, 9397–9406 (2010).
16. Dhawan, A. *et al.* Focused ion beam fabrication of metallic nanostructures on end faces of optical fibers for chemical sensing applications. *J. Vac. Sci. Technol. B* **26**, 2168–2173 (2008).
17. Ma, X. *et al.* Surface-Enhanced Raman Scattering Sensor on an Optical Fiber Probe Fabricated with a Femtosecond Laser. *Sensors* **10**, 11064–11071 (2010).
18. Lan, X. *et al.* Surface-enhanced Raman-scattering fiber probe fabricated by femtosecond laser. *Opt. Lett.* **34**, 2285–2287 (2009).
19. Lindroos, S. & Leskelä, M. in *Solution Processing of Inorganic Materials* (ed Mitzi, D.) 239–270 (Wiley, New Jersey, 2009).
20. Potiyaraj, P., Kumlangdudsana, P. & Dubas, S. T. Synthesis of silver chloride nanocrystal on silk fibers. *Mater Lett* **61**, 2464–2466 (2007).
21. Le Ru, E. C., Blackie, E., Meyer, M. & Etchegoin, P. G. Surface enhanced Raman scattering enhancement factors: a comprehensive study. *J. Phys. Chem. C* **111**, 13794–13803 (2007).
22. Efremov, E. V., Ariese, F. & Gooijer, C. Achievements in resonance Raman spectroscopy review of a technique with a distinct analytical chemistry potential. *Anal. Chim. Acta* **606**, 119–134 (2008).
23. Carpenter, A. E. *et al.* CellProfiler: image analysis software for identifying and quantifying cell phenotypes. *Genome Biol.* **7**, R100; doi:10.1186/gb-2006-7-10-r100 (2006).
24. Hastie, T., Tibshirani, R. & Friedman, J. in *The Elements of Statistical Learning* [191–218] (Springer, New York, 2009).

## Acknowledgments

This work was supported by the Academy of Finland (Grant no. 247092, Grant no. 126576, Grant no. 284909) and the Finnish Funding Agency for Technology and Innovation (TEKES, Grant no. 70011/12).

## Author contributions

A.M. performed the measurements, imaging and data processing. T.N., P.V. and S.H. supervised the work. All authors read and approved the final manuscript.

## Additional information

**Supplementary information** accompanies this paper at <http://www.nature.com/scientificreports>

**Competing financial interests:** The authors declare no competing financial interests.

**How to cite this article:** Matikainen, A., Nuutinen, T., Vahimaa, P. & Honkanen, S. A solution to the fabrication and tarnishing problems of surface-enhanced Raman spectroscopy (SERS) fiber probes. *Sci. Rep.* **5**, 8320; DOI:10.1038/srep08320 (2015).



This work is licensed under a Creative Commons Attribution-NonCommercial-ShareAlike 4.0 International License. The images or other third party material in this article are included in the article's Creative Commons license, unless indicated otherwise in the credit line; if the material is not included under the Creative Commons license, users will need to obtain permission from the license holder in order to reproduce the material. To view a copy of this license, visit <http://creativecommons.org/licenses/by-nc-sa/4.0/>